European Journal of Soil Science, Volume 72, Issue 1, January 2021, pp. 141-153
DOI:10.1111/ejss.12975

Influence of soil structure on the spread of *Pseudomonas fluorescens* in soil at microscale

Running title: Spread of *Pseudomonas fluorescens* in soil

Archana Juyal[1, 2, 3], Wilfred Otten[1, 4], Philippe C. Baveye[5], Thilo Eickhorst[2*]

[1] School of Science Engineering and Technology, Abertay University, Dundee, UK.

[2] FB 2 (Biology/Chemistry), University of Bremen, Bremen, Germany.

[3] Department of Plant, Soil and Microbial Sciences, Michigan State University, Michigan, USA.

[4] School of Water, Energy and Environment, Canfield University, Cranfield, UK.

[5] ECOSYS Unit, AgroParisTech, Université Paris-Saclay, Avenue Lucien Brétignières, 78850 Thiverval-Grignon, France.

Abstract

For over a half a century, researchers have been aware of the fact that the physical and chemical characteristics of microenvironments in soils strongly influence the activity, growth, and metabolism of microorganisms. However, many aspects of the effect of soil physical characteristics, such as the pore geometry, remain poorly understood. Therefore, the objective of the present research was to determine the influence of soil pore characteristics on the spread of bacteria, observed at the scale relevant to microbes. *Pseudomonas fluorescens* was introduced in columns filled with 1-2 mm soil aggregates, packed at different bulk densities. . Soil microcosms were scanned at 10.87 µm voxel resolution using X-ray computed tomography (CT) to characterize the

* Corresponding author. E-mail: eickhorst@uni-bremen.de

geometry of pores. Thin sections were prepared to determine the spread and colonization of bacteria. The results showed that average bacterial cell density was 174 cells mm^{-2} in soil with bulk density of 1.3 g cm^{-3} and 99 cells mm^{-2} in soil with bulk density of 1.5 g cm^{-3}. Soil porosity and solid-pore interfaces influence the spread of bacteria and their colonization of the pore space at lower bulk density, resulting in relatively higher bacterial densities in larger pore spaces. The study also demonstrates that thin sectioning of resin impregnated soil samples can be combined with X-ray CT to visualize bacterial colonization of a 3D pore volume. This research therefore represents a significant step towards understanding how environmental change and soil management impact bacterial diversity in soils.

Keywords

Bacterial spread; pore geometry; soil thin sections; X-ray computed tomography; fluorescence microscopy

Highlights

- We used a quantitative approach to study bacterial spread in soil at scales relevant to microbes.
- The rate of pseudomonas spread decreased with increased bulk density of soil.
- Soil porosity and soil-pore interface influence pseudomonas in lower bulk density soil.
- Soil structure with different pore characteristics effects spread and activity of bacteria in soil.

1 Introduction

Soil microorganisms are intimately involved in numerous processes occurring in soils, including the supply of nutrients to plants, the stimulation of plant growth through production of growth hormones, controlling the activity of plant pathogens, maintaining soil architecture, and contributing to the leaching of inorganics and the mineralization of organic pollutants (Baveye et al., 2018; Burd, Dixon, & Glick, 2000; Hayat , Ali, Amara, Khalid, & Ahmed, 2010; Zaidi, Khan, Ahemad, & Oves, 2009; Zhuang, Chen, Shim, & Bai, 2007). These microbial communities have immense metabolic and physiological heterogeneity, which enables them to live, adapt, and proliferate in soil environments that also exhibit an extremely high level of structural and chemical heterogeneity (Madigan, Clark, Stahl, & Martinko, 2010). Despite the relatively high bacterial abundance in fertile soil, bacteria occupy only a small fraction of the soil surfaces (Young, Crawford, Nunan, Otten, & Spiers, 2008). In soil, microorganisms tend to aggregate (Ekschmitt, Liu, Vetter, Fox, & Wolters, 2005), forming microbial hotspots in very small volumes of soil (<1 cm^3). In a review, Kuzyakov and Blagodatskaya (2015) argue that most of the biogeochemical processes are taking place in these hotspots. Such hotspots are transient in nature and originate from complex interactions between physical, chemical and microbial processes. Examples of such hotspots of activity include the rhizosphere, the detritus-sphere, and the surface of soil aggregates. Of these examples of hotspots, the rhizosphere is the most dynamic with hotspots lasting days, whereas hotspots associated with soil structure can be more persistent and last for months.

Hotspots of microbial activity do not exist in isolation. A co-location of various conditions is required for the aforementioned processes to occur. Soil pores

play a significant role in formation of such hotspots as soil architecture forms an interconnected network through which various processes including diffusion of oxygen, transport of enzymes and dissolved organic matter, mobility of bacteria, and interaction between bacterial species occur. A number of researchers have observed spatial patterns in the distribution of bacteria at a microhabitat scale (Vieublé Gonod, Chadoeuf, & Chenu, 2006; Kizungu et al., 2001; Nunan, Wu, Young, Crawford, & Ritz, 2003). For example, Vieublé Gonod et al. (2006) observed a heterogeneous pattern of mineralization of 2,4-D (2,4 Dichlorophenoxyacetic acid) in a soil, with an increase in variability when going from field- to microhabitat scale. An explanation is that bacteria are not randomly distributed and are located in different microenvironments (i.e. mainly located in pores of different size and shapes) in soil.

Despite that soil structure plays a regulating role in most of these processes, studying of these processes at microscale is hampered by the opacity of soils and inability of single technology to visualise all processes that are involved. As such we have little knowledge about movement by bacteria from a local micro-site in soil and how this is affected by physical characteristics such as pore structure. It is essential to understand the exact mechanisms that are involved in microbial processes (e.g. hotspots occurrence) in order to predict its cumulative effect at large scale. No single technology is available to address this issue, but it could be addressed through the application of multiple techniques to bring together physical, chemical and biological characterisation. The merging of various technologies has received great attention in the recent years (Baveye et al., 2018; Hapca, Baveye, Wilson, Lark, & Otten, 2015; Juyal et al., 2019; Schlüter et al., 2018).

In this study we apply such integrative imaging approaches to study how bacteria move in soil and how soil structure regulates the spatial distribution of bacteria. Our key objective is to analyse the influence of soil architecture on the extent of spread of bacteria in soil from a localised spot at the microscale. We investigated this by quantifying the spatial distribution of *Pseudomonas fluorescens* following introduction into microcosms with controlled structural properties by examining soil thin sections and quantifying the characteristics of soil pore space using X-ray CT. Through X-ray CT we determine pore space characteristics like porosity, which quantifies the total volume available to microbial interactions and growth, the connectivity of pores, which indicates how accessible the pore volume is for organisms to interact and find food sources, and the pore-solid interface area, which effectively defines the surface area accessible to microorganisms in soils.

This allowed us to test the following hypothesis related to the impact of soil structure on spatial distribution of bacteria in soil:

1. bacterial densities increases in a small volume surrounding nutrient sources.
2. the extent of high bacterial density around nutrient sources reduces with increasing bulk density due to reduced mobility and diffusion.
3. soil porosity, pore connectivity and soil-pore interface influence the spread and colonisation of bacteria.

2 Materials and Methods

2.1 Soil Sampling and preparation

Soil samples used in this study originated from a sandy loam soil collected in 2011 at an experimental site, Bullion field, situated within the James Hutton Institute in Invergowrie, Scotland. The soil was air-dried, and soil aggregates

were sieved down to an aggregate size of 1-2 mm and stored in a cold room (4°C). The physicochemical characteristics of the selected soil aggregate fraction (1-2 mm) are as follows: Sand, 55.7%; Silt 31.0%; Clay, 13.3%; Organic matter, 5.5%; C/N ratio, 17.1. For the experiment, the soil was sterilized by autoclaving twice (moist heat) in glass bottles at 121°C at 100 kPa for 30 minutes with a 24 h interval time. The aggregate size of 1-2 mm was selected based on a previous study (Juyal et al., 2018).

2.2 Pseudomonas fluorescens inoculum preparation

Pseudomonas fluorescens cells (SBW25) were used as bacterial inoculum. *Pseudomonas* was grown on King's B medium (KB, 10 g Glycerol, 1.5 g K_2HPO_4, 1.5 g $MgSO_4.7H_2O$, 20 g Proteose peptone No.3 (Becton, Dickinson & Company, UK), 15 g Technical agar (1.5 % w/v) per litre) (King et al., 1954).

For each experiment, an overnight culture was prepared by transferring a loop-full of colony in 10 mL of sterile broth and incubated at 28°C on a shaker at 200 rpm for 24 h. The cells were harvested by centrifugation (4,000 × g) for 5 min and re-suspended in 10 mL PBS solution to a final concentration of OD_{600} = 0.95.

To provide a reproducible source of inoculum to introduce bacteria in the soil, an agarose pellet was used as described in Juyal et al. (2018). Briefly, a 1000 µL inoculum of washed cells (see above) was mixed with 30 mL of 1.5% LMP agarose solution (Fisher bioregaents, UK; geling point ≤35°C). After pouring a layer of approx. 2 mm height in a sterile petri dish, sterile glass beads (2 mm in diameter) were sparsely placed on the solidified agarose. Subsequently they were covered by additional agarose to a final height of 5 mm. The solidified agarose was then cut into small cylindrical shaped pellets (referred as inoculum

155 pellet) using the circular end of a 1 mL pipette tip. Each pellet was 3.5 mm in
156 diameter and ca. 4 mm in height and contained a glass bead in its centre
157 (Figure_1_Supp). The glass beads were used to ensure that the location of
158 inoculation could be identified via X-ray CT scanning and in soil thin sections.
159 Control pellets without bacteria were prepared in a similar way.
160

161 *2.3 Preparation of soil microcosms*

162 The effect of structure on the spread of bacteria was studied by preparing
163 microcosms in polyethene rings of size 3.4 cm^3 (inner diameter 17.0 mm and
164 height 15.0 mm) packed at two soil bulk densities, 1.3 and 1.5 g cm^{-3}. Previous
165 work showed that these densities give significant differences in pore geometry
166 (Juyal et al., 2019). The moisture content of the soil was adjusted to 60% pores
167 filled with water for all samples. The amount of water added to soil to acquire 60%
168 water filled pores was 0.224 $cm^3\ g^{-1}$ for bulk density of 1.3 g cm^{-3} and 0.1569 $cm^3\ g^{-1}$
169 for bulk density of 1.5 g cm^{-3}. The total porosity of soil at bulk density of 1.3 g
170 cm^{-3} was 48% and 40% for soil packed at bulk density of 1.5 g cm^{-3}.
171 Soil was transferred in these rings in two layers, covering half the height each.
172 After packing the bottom half of the soil, an inoculum pellet was placed on top
173 of the soil layer in its centre and then covered with the second half of soil.
174 Control samples with the sterile inoculum pellet were packed in a similar way.
175 Three replicates per treatment were prepared, producing 12 soil microcosms in
176 total. The microcosms were incubated at 23°C in the dark to allow bacteria to
177 grow and spread in soil. The soil microcosms were sampled after an incubation
178 period of 14 days.
179

2.4 *Impregnation of soil microcosms*

The impregnation of soil microcosms was done according to the protocol of Juyal et al. (2019). Briefly, the samples were fixed overnight with 2% formaldehyde solution (v/v in H_2O; 37% stock solution, Sigma Aldrich) at 4°C. The samples were washed in MQ distilled water and dehydrated with a graded series (50, 70, 90 and three changes of 100%) acetone (technical grade, VWR) to avoid interference with the polymerization of resin. The acetone saturated samples were kept under vacuum (280 mbar) to facilitate the entire exchange of all pores.

An impregnation mixture (2 L) was prepared by amending 1.4 L of polyester resin (Palatal P50-01, Büfa, Germany) with 2,240 µL of Co-accelerator (1.6‰ (v/v) 1%-Cobalt Octoate accelerator, Oldopal, Büfa, Germany) and 4,480 µL of hardener (3.2‰ (v/v) cyclohexanone peroxide, Akzo Nobel, Germany). After amending 500 mL of acetone were added as a thinner, mixed well and the resin mixture was kept under vacuum (240 mbar) to remove gas bubbles before adding it to the samples. Acetone was removed from the container with samples which were subsequently transferred into a desiccator equipped with a tube and a valve connected to the resin mixture. The resin mixture was added slowly under vacuum (240 mbar) to allow an infiltration of microcosms with resin from the bottom to the top to ensure that the pores of the soil were filled with resin mixture as completely as possible. Shortly before reaching the surface of the microcosms (after approx. 45 min) the addition of resin was stopped for a while and vacuum was increased (200 mbar) for 1 h to remove the gaseous phase from the soil pores carefully. Finally, the remaining mixture was added to cover the samples completely with resin. Samples were left at

205 room temperature under a hood for polymerization of the resin which lasted
206 nine days.
207 After polymerization, excess resin and the PE rings of samples were removed to
208 produce a cylindrically shaped resin impregnated soil sample. A straight vertical
209 cut was made on the edge of each sample using a diamond saw (Woco 50,
210 Conrad, Germany) to ensure the starting point of the scan is the same for all
211 samples while scanning under X-ray CT.
212

213 *2.5 X-ray CT scanning of impregnated microcosms*

214 The impregnated samples were scanned using a Metris X–Tek HMX CT
215 scanner. Samples were scanned at 10.87 µm voxel resolution with energy
216 settings of 200 keV and 56 µA and 2000 angular projections. The straight
217 vertical cut was used as a reference side facing the gun of the CT scanner for
218 each scan to facilitate alignment for image processing. A tungsten target with a
219 0.25 mm aluminium filter was used. Reconstruction of radiographs into 3D
220 volumes was done using Metris X-Tek software CT Pro v2.1 (NIKON metrology,
221 Tring, UK). A volume processing software VGStudio MAX V2.2 (Volume
222 graphics, Heidelberg, Germany) was used to change contrast in reconstructed
223 volumes and to export image stacks (*bmp format) for further processing.
224

225 *2.6 Preparation of soil thin sections*

226 After X-ray CT scanning, three soil thin sections were prepared for cell counting
227 from each individual resin impregnated soil microcosm. One thin section passed
228 through the centre of the glass bead and the others approx. 2.5 mm away from
229 the bead (Figure_2_Supp). To prepare soil thin sections, the reference side of
230 the soil block (opposite side of the vertical cut described above) was glued onto

231 a petrographic slide of size 27 x 46 mm and thickness 0.15 mm (Beta diamonds
232 Inc, CA, USA) with epoxy resin (Epofix resin, Struers, Denmark). An estimated
233 distance of each thin section from the reference slide was calculated by
234 measuring the distance between the reference side and the glass bead in X-ray
235 CT grey scale images. Samples were cut and polished using a diamond coated
236 saw and cupwheel grinder (Discoplan TS, Struers). A frosted petrographic slide
237 was glued on the polished surface of the sample. Subsequently the opposite
238 side of the sample was cut and the sample was polished to a final thickness of
239 approx. 30 µm.
240 The final thickness of each thin section was measured with a micrometer (1 µm
241 accuracy) considering the thickness of the slide and the amount of glue added.
242 The measured values were used to determine the exact position of the prepared
243 soil thin sections within the scanned sample. The thin sections were referred to
244 as II (through centre of bead), I and III (approximately 2.5 mm above and below
245 the bead towards the reference side respectively).
246

247 *2.7 Enumeration of bacteria in soil thin sections*

248 For enumeration of bacterial cells, a drop of mounting medium containing 1.5 µg
249 mL^{-1} of DAPI stain (Vectashield H-1200, Vector Laboratories, CA, USA) was
250 applied on top of the soil thin sections and covered with a cover slip of size 27 ×
251 46 mm (Beta diamonds Inc, CA, USA). Bacterial cells were observed with an
252 Olympus BX61 fluorescence microscope (Olympus, Japan) equipped with a 100
253 W Hg vapour lamp (HBO 102 W/2, Osram, Germany), using a 100× objective
254 lens (UPlanSApo, Olympus, Japan). DAPI stained bacterial cells were observed
255 under UV excitation (filter set U-MWU2, Olympus, Japan) and counted manually

using a reticule grid (10 × 10, 12.5 mm; Spectra Services, NY, USA) in a 10× eyepiece (WHN10×, Olympus, Japan).

Slides with soil thin sections were placed in a horizontal position and the scale of the microscope stage was used in order to be able to start, and revisit, from the same spot in each parallel soil thin section for better alignment. Cell counts were obtained on counting spots following five lines on each thin section. The first counting line was based on the centre of the glass bead followed by two lines above and below the first line at a distance of 1 mm respectively (Fig. 1). Four fields of view (henceforth referred as analysed spot) of size 250 µm × 250 µm were counted per spot. The distance between each analysed spot was 1 mm. In total 9 spots per line were analysed on each thin section. The cell counts were extrapolated to cell density i.e. cell counts per area of the counting spot.

To compare the proportion of bacteria determined in thin sections with general cell numbers per g of bulk sample, an additional set of samples were prepared in a similar way as described in section 2.3. The cells were enumerated in dispersed soil samples according to the protocol described by Juyal et. al 2018. Briefly, soil microcosms were suspended in 10 ml of 1× PBS solution. 500 µl of the suspension was fixed in 4 % formaldehyde solution in 1× PBS at 4°C for 2.5 hours. The samples were filtered on a polycarbonate filter membrane for performing CARD-FISH. The filter sections were hybridized with HRP-labelled oligonucleotide probes. After hybridization, for tyramide signal amplification the filter sections were incubated with the amplification buffer containing fluorescein-labelled tyramides. After amplification the filter sections were washed in distilled water (dH_2O) and dehydrated with ethanol. The filter sections were mounted with an antifading solution containing DAPI stain on glass slides. The CARD-FISH signals were detected on filter sections under

282 epifluorescence microscopy with a double excitation filter set (#24, Carl Zeiss,
283 Oberkochen, Germany).
284
285 *2.8 Image processing and analysis of pore geometry*
286 For image processing a stereomicroscopic image of each soil thin section was
287 taken and used to retrieve the same layer from the image stacks of CT data
288 (Fig. 2). The distance of each thin section from the reference side measured
289 was also used. The selected CT image was then cropped to the region of
290 interest of size 1.0 × 1.0 mm (the area where bacterial cells were counted). The
291 cropped region of interest of each thin section was then thresholded using an
292 in-house developed indicator kriging method (Houston, Otten, Baveye, &
293 Hapca, 2013a).
294 The pore geometry of each soil thin section was analysed at smaller scale in 3D
295 as described in Juyal et al. (2019). Briefly, the neighbouring slices above and
296 below the selected region of interest (each analysed spot) were considered and
297 cropped down to 1 mm size. In-house developed software was used to quantify
298 porosity, connectivity and solid-pore interfacial area of the pores, based on
299 voxel data obtained from CT-scans (detection limit of 10.87 µm). The porosity
300 was calculated as the volume fraction occupied by pores, whereas connectivity
301 was determined as the volume fraction of pore space that is connected with the
302 external surface of the image volume. The surface area of solid-pore interfaces
303 was estimated using Minkowski functionals, and expressed in relation to the
304 area of solids directly connected to the pore space (Houston et al., 2013b).
305

306 *2.9 Statistical analysis*

307 Statistical analysis was performed using SPSS version 22. A mixed effect linear
308 model (assuming normal distribution) was used to investigate differences in soil
309 pore characteristics for different treatments, with treatments as fixed factor. The
310 data were assessed for normality first using Shapiro-Wilk test and secondly by
311 observing normal probability plots and histograms using SPSS. To comply with
312 the normality assumption the porosity and connectivity measures were
313 transformed using the probit function. The solid-pore interfacial area data met
314 the normality assumption; hence they did not require any preliminary
315 transformation.

316 A generalised mixed effect Poisson model with log link function was used to
317 investigate significant difference in bacterial cell density between different
318 treatments with soil thin sections and treatments as fixed factors. The effect of
319 soil structure properties such as porosity, connectivity and solid-pore interfacial
320 area on the extent of spread of bacteria was also analysed by a Poisson model
321 with treatments and thin sections as fixed factors. The size of each analysed
322 spot was introduced as an offset variable in the Poisson model.

323 Statistical analysis of total cell counts in soil thin sections and soil suspensions
324 was done by a Tukey HSD post-hoc test.

325

326

327 **3 Results**

328 *3.1 Pore characteristics of soil microcosms*

329 The pore characteristics of the two bulk density treatments differed in terms of
330 porosity, connectivity and solid-pore interfacial area (Table_1_Supp). The
331 analysis of soil porosity indicated that soil packed at bulk density of 1.3 g cm^{-3}

had an average porosity of 24% (SE ±1.05%) compared to 23% (SE ±0.91%) for soil packed at higher bulk density of 1.5 g cm^{-3}, however the difference was not statistically significant (p=0.612) which may be a result of the limited resolution in X-ray CT scanning (see 4.1). The difference between the two bulk density treatments in terms of the connectivity of pores was statistically significant (p=0.0456), with an average connectivity of pores from 94% (SE ±0.55%) for soil packed at the lower bulk density to 89% (SE ±0.99%) for soil packed at higher bulk density. The solid-pore interfacial area declined with increasing bulk density from 0.05 mm^2 (SE ±0.001 mm^2) in soil packed at bulk density of 1.3 g cm^{-3} to 0.04 mm^2 (SE ±0.001 mm^2) in soil packed at bulk density of 1.5 g cm^{-3} (p=0.000).

3.2 Enumeration of Pseudomonas cells in soil thin sections

Pseudomonas cells stained with DAPI appeared bright blue in colour against a brown coloured soil background (Fig. 3). The *Pseudomonas* cells were mainly observed within the soil matrix or at solid-pore interfacial area representing internal aggregate structures and aggregate surfaces respectively. In the lower bulk density treatment the bacterial cells appeared to be in form of small group of colonies (Fig. 3A), compared to the higher bulk density treatment (Fig. 3B). The autofluorescence of some soil compounds did not hamper the enumeration of bacterial cells as they appeared yellowish in colour. Both the treatments showed a substantial variability in the bacterial cell counts at microscale (Fig. 4). *Pseudomonas* cells ranged from 0 to 33 cells per analysed spot in soil with lower bulk density and from 0 to 23 cells per analysed spot in soil with higher bulk density. In control samples, bacterial cells ranged from 0 to 11 in soil with a low bulk density and 0 to 6 in soil with a high bulk density (Figure_5_Supp).

358 Most analysed spots were observed to be completely devoid of cells. The
359 proportion of analysed spots without cells was greater in soil packed at bulk
360 density of 1.5 g cm^{-3} compared to soil packed at a bulk density of 1.3 g cm^{-3}.
361 The average cell density of *Pseudomonas* cells was 42% higher in soil with
362 lower bulk density (p<0.001) with 174 cells mm^{-2} (SE ±6.3), compared to soil
363 packed at the higher bulk density which had a bacterial density of 99 cells mm^{-2}
364 (SE ±4.3). In control samples, bacterial cell density was 26 cells mm^{-2} (SE ±4.3)
365 for soil packed at bulk density of 1.3 g cm^{-3} and 14 cells mm^{-2} (SE ±1.1) for soil
366 packed at bulk density of 1.5 g cm^{-3}. Although some bacterial cells were
367 observed in control samples of both the treatments, the difference between the
368 control and inoculated samples was statistically significant (p<0.001).
369 The spread rate of *Pseudomonas* at different distances from the inoculum point
370 in soil was affected in both the treatments (Fig. 5). The average cell density at
371 given distance from the inoculum point was higher (β=3.122) for the soil packed
372 at lower bulk density. Overall, the rate of *Pseudomonas* spread at any given
373 distance from the inoculum point was significantly (p=0.002) higher in soil
374 packed at lower bulk density compared to soil packed at higher bulk density
375 (p=0.447). These results confirm that *Pseudomonas* cells dispersed further
376 from the inoculation point source in soils packed at bulk density of 1.3 g cm^{-3}
377 compared to soil packed at bulk density of 1.5 g cm^{-3}.
378 Cells enumerated on soil thin sections were extrapolated to cells g^{-1} of soil and
379 compared with cell numbers obtained from dispersed samples. In soil packed at
380 lower bulk density respective cell counts were 1.32×10^{8} (SE ±1.60×10^{7}) cells g^{-1}
381 of soil in dispersed samples and 1.34×10^{8} (SE ±2.25×10^{7}) cells g^{-1} of soil in
382 thin sections. In soil packed at higher bulk density cell counts were 7.62×10^{7}

383 (SE ±8.41×10^6) cells g^{-1} of soil in dispersed samples and 6.62×10^7 (SE
384 ±1.12×10^7) cells g^{-1} soil in thin sections (Figure_3_Supp and Figure_4_Supp).
385
386 *3.3 Pore geometry influence on the extent of Pseudomonas spread in soil*
387 In Fig. 6, the relationships between the soil pore characteristics and bacterial
388 cell density in each analysed spot of the analysed soil thin sections in both bulk
389 density treatments are presented. The influence of soil pore characteristics on
390 the spread of *Pseudomonas* cells differed in soil packed at lower bulk density
391 compared to soil packed at higher bulk density (Table 2). A contrasting
392 influence of soil porosity on the spread of bacteria was observed between the
393 two treatments, with a decrease in cell density (β=-1.453) in lower bulk density
394 and an increase in cell density (β=1.225) in higher bulk density treatment.
395 However, the influence was not statistically significant in both the treatments.
396 Solid-pore interfacial area significantly influenced the spread rate of
397 *Pseudomonas* cells in lower bulk density treatment. An increase (β=5.999) in
398 cell density was observed with greater solid-pore interfacial area (>0.03 mm^2).
399 A slight increase in the cell density (β=1.034) with increasing solid-pore
400 interfacial area was also observed in soil packed at higher bulk density
401 samples, however the influence was not statistically significant.
402 The connectivity of pores showed significant influence on the spread of bacteria
403 only in samples packed at lower bulk density, with a slight decrease in cell
404 densities (β=-3.274) with decreasing connectivity of pores (Fig. 6c).
405
406

4 Discussion

In this paper a methodological approach developed in our previous paper (Juyal et al., 2019) was used to investigate the influence of soil pore characteristics on the spatial spread of bacteria from localised nutrients in soil. The introduction of bacteria in the form of an agarose pellet into soil is proposed as way to introduce bacteria in solid form compared to the liquid inoculum method used in our previous paper (Juyal et al., 2019). The reason is that an addition of liquid suspension of bacterial inoculum would influence spread of introduced bacteria in soil, water movement would occur and lead to redistribution of bacteria immediately after introduction in soil. Another advantage of using the solid form is that it provides a reproducible source of inoculum. The introduction of a localised source of inoculum resulted in dispersion of bacteria into the soil largely due to bacterial movement and growth.

4.1 Enumeration of bacteria in soil thin sections

A difference in cell densities during the 14 days of incubation was observed between the two different bulk density treatments. The detection of bacterial cells in the soil thin sections evidently showed the colonization and spread of bacteria in the surrounding soil area away from the inoculation point. A plausible explanation for this is that *Pseudomonas* spread towards nutrients present in the surrounding areas, as the source of inoculation was nutrient poor compared to the soil. The range of cell counts varied at different distances from the inoculation point. This could be due to the concentration of nutrients available in different regions of soil, e.g. nutritional heterogeneity at microscopic scales, but it may also reflect different pathways for spread. Gupta Sood (2003) showed higher numbers of *Pseudomonas fluorescens* cells attracted towards

433 substances exuded by vesicular-arbuscular mycorrhizal roots compared to non-
434 vesicular arbuscular mycorrhizal roots. Some other studies (de Weert et al.,
435 2002; Neal, Ahmad, Gordon-Weeks, & Ton, 2012) have observed similar higher
436 response of *Pseudomonas* spp. towards substances or metabolites from root
437 exudates of tomato and maize plants.
438 The average cell density showed high variability in the spread of bacteria at
439 different distances from the inoculation point. The cell density was higher in the
440 thin section closer to the inoculation point compared to the other one (2.5 mm
441 away) in both the bulk density treatments. This is likely due to the distance to
442 access nutrients in soil was shorter in the thin section closer to the inoculation
443 point compared to the other thin section that was further away.
444 A study by Nunan, Wu, Young, Crawford and Ritz (2002) showeda high degree
445 of aggregation of bacterial cells in topsoil compared to subsoil. In the present
446 study, the distances between the two sections refers to the different depth of
447 soil. The nutrient distribution between these two thin sections is relevant to the
448 availability of nutrients found in the field soil. Another study by Dechesne,
449 Bertolla, Grundmann, Lyon and Icrobiol (2005) also showed a high variation in
450 the distribution of introduced bacteria *Pseudomonas putida* after addition of
451 substates to soil columns. The length of incubation time can also be another
452 reason for such distribution patterns of bacteria in soil. By the time the
453 microcosms were sampled bacteria would have grown and colonised in the soil
454 closer to the inoculation point (represented by the thin section in the centre of
455 the sample) more than the other sections.
456 Growth of introduced *Pseudomonas* cells in soil columns was confirmed by
457 comparing CARD-FISH cell counts in dispersed samples taken 1 and 14 days
458 after inoculation respectively. Number of DAPI cell counts analysed on soil thin

459 sections was verified by cell enumeration using CARD-FISH (Schmidt,
460 Bengough, Gregory, Grinev, & Otten, 2012) on a set of microcosms which was
461 incubated in parallel. Cell numbers were in the same range and thus staining
462 and counting using DAPI on polished resin impregnated samples has proven to
463 be efficient (Figure_3_Supp). Bacterial numbers analysed (by CARD-FISH) in
464 dispersed samples of both treatments showed an increase in cell counts on day
465 14 compared to day 1. For example, *Pseudomonas* cell counts increased from
466 3.62×10^{7} (SE $\pm3.88\times10^{6}$) on day 1 to 1.32×10^{8} (SE $\pm1.60\times10^{7}$) on day 14 for
467 samples packed at bulk density of 1.3 g cm^{-3} (Figure_4_Supp).
468 Among the two treatments, the hypothesis that increasing bulk density would
469 affect the spread rate of bacteria in soilwas confirmed, and a decrease in the
470 spread of bacteria with increasing bulk density was observed. These results are
471 consistent with the findings of our previous work, which showed a decrease in
472 the rate of spread with increasing bulk density over time. The difference in cell
473 density could be due to the alterations in soil pore geometry which limited the
474 access of bacteria to nutrients in soil as the number of bacteria added in both
475 treatments was the same.
476 The pore characteristics of each analysed spot where bacteria were counted
477 was also analysed. Results showed that only connectivity and solid-pore
478 interfacial area of pores were affected by increasing bulk density. Soil porosity
479 determined by X-ray CT was quite similar for both bulk density treatments. This
480 may be because the pores analysed here were limited to the scanning
481 resolution i.e. only pores greater than 10.87 µm were analysed. For example,
482 the total porosity of a sample packed at bulk density of 1.3 g cm^{-3} is 48 % and
483 of soil packed at bulk density of 1.5 g cm^{-3} is 40% (calculated based on bulk
484 density and particle density). However, the porosity determined by X-ray CT

485 scanned at a resolution of 10.87 µm resulted in 24% for soil packed at a bulk
486 density of 1.3 g cm^{-3} and 23% for soil packed at bulk density 1.5 g cm^{-3}. This
487 means that around 42-50% of the total porosity is not detected by the scanner.
488 Therefore, the conclusions made in this study on the pore characteristics are
489 based on the pores greater than the detection limit.
490 However, the pores analysed are more relevant to the present study as the
491 larger pores will affect the distribution of water and the air-water interface, the
492 diffusion pathways of dissolved organic carbon and the diffusion pathways of
493 oxygen and hence can be expected to affect the growth and spread of bacteria
494 in different treatments. Moreover fine micropores (≤0.2 µm in diameter) are less
495 relevant for this study as they represent non-habitable pore space (Hassink,
496 Bouwman, Zwart, & Brussard, 1993). As these pores are estimated to account
497 for 14% and 12% at 1.3 g cm^{-3} and 1.5 g cm^{-3} bulk density respectively (Ad-
498 hoc-AG Boden, 2005), only 5-10% of the pores being relevant for this study
499 could not be detected via CT. This is consistent with the study by Juyal et al.
500 (2018) who showed that the larger pores determined by X-ray CT had a
501 significant impact of the growth and spread of bacteria.

502 *4.2 Influence of pore characteristics on Pseudomonas spread*

503 To investigate if the pore geometry did influence the spread rate of bacteria in
504 soil, pore characteristics of each analysed spot were analysed at microscale.
505 Soil porosity did not show a significant influence on the extent of *Pseudomonas*
506 spread in soil. This could be because of the scale of observation with X-ray CT
507 which visualises pores that were air-filled prior to resin impregnation whereas
508 the majority of bacteria are located in pores that were water filled respectively.
509 The connectivity of pores showed significant influence on the spread of bacteria
510 only in loosely packed soil. A decrease in connectivity of pores with increase in

511 bulk density could have resulted in limited access to nutrients, water movement
512 and gas exchange.
513 In a few analysed spots bacterial cells were observed in 0% connected pores.
514 As connectivity is required for bacteria to move, it is most likely that these pores
515 are connected through pores below the scanning resolution, but large enough
516 for bacteria to move through. Therefore, to avoid biased results we excluded
517 the cell count data observed at 0% connected pores. A significant influence of
518 solid-pore interfacial area of pores on bacterial cell spread rate was observed in
519 the lower bulk density treatment. A plausible explanation for this is that at lower
520 bulk density nutrients might have been readily accessible to bacteria as they
521 are transported through soil and, therefore, bacteria might have colonised near
522 the vicinity of these pores. This may also be that in partially saturated soil water
523 is retained on the surfaces as thin films to accommodate introduced bacterial
524 cells Carminati, Kaestner, Lehmann and Flühler (2008). In addition, bacteria
525 tend to grow on the surfaces of substrates as can be seen from the soil thin
526 sections (Fig. 3). The consequence of this result is that if pore geometry affects
527 the spread and colonisation of bacteria at microscale, it will also affect the
528 activity of microbes in soil. This shows that the pore characteristics control the
529 access of nutrients in soil. Strong, De Wever, Merckx and Recous (2004)
530 showed that the rate of decomposition of organic C depends on the location in
531 the soil pore network. Ruamps, Nunan and Chenu (2011) also showed that
532 decomposition of organic carbon and microbial community structure varies in
533 pores of different size classes in soil. In the present study some of the soil pore
534 characteristics like porosity and solid-pore interfacial area showed significant
535 influence on the extent of bacterial spread in soil at microscale.

Thus, the method developed in the present study can be used to study how introduced bacteria contact their target through soil to carry out activities like promoting plant growth or mineralization of soil pollutant. The study highlights how the physical factors (bulk density in this case) expected to influence the distribution of microorganisms at macroscopic scales varies at microscopic scale. Therefore, this study shows the importance of studying the parameters affecting at activity of microorganisms in soil at scale relevant to microbes.

5 Conclusion

In this study, we provide evidence that bacteria spread though soil in absence of water movement. We also showed that soil physical conditions and pore architecture in particular affect the rate and extent of spread of bacteria through soil. The rate of spread of *Pseudomonas* bacteria was faster in soil packed at lower bulk density compared to soil packed at higher bulk density. Analysis of X-ray CT images of soil thin sections of samples packed at lower and higher bulk density revealed that the rate of spread of bacteria was influenced by connectivity of soil pores and solid-pore interfacial area at the lower bulk density. This study thus suggests that soil structure can affect the growth and spread of bacteria and thus their activity. Information collected from this methodological approach can be used to build mathematical models to explore the link between microbial community activities and various soil parameters, such as explored by Portell, Pot, Garnier, Otten and Baveye (2018). Further research is therefore required to study the complete effects of physical, chemical, and biological properties on the microbial processes in soil for better soil management.

562

563

564 **Acknowledgements**

565 This research was made possible in part through the financial support provided
566 to PCB by the Kodak endowment at the Rensselaer Polytechnic Institute (RPI,
567 Troy, New York), which allowed AJ and TE to spend time at RPI to conduct
568 experiments. AJ acknowledges support from SORSAS and DAAD
569 (A/12/76235). WO received funding from the Natural Environment and
570 Research Council (NE/P014208/1). TE received funding from the University of
571 Bremen (ZF/02/600/10). We thank Dr. Stefan Knauth for his advice and
572 assistance for the preparation of the inoculum.

573

574 **ORCID: 0000-0003-0436-9895**

575 **Data Availability Statement**

576 The underlying data can be accessed through the Cranfield University data
577 repository at http://doi.org/10.17862/cranfield.rd.11854239

578 **Conflict of Interest**

579 None

580 **References**

581 Ad-hoc-AG Boden (Ed.). (2005). *Bodenkundliche Kartieranleitung*. 5th ed.
582 Stuttgart: E. Schweizerbart'sche Verlagsbuchhandlung.
583 Baveye, P. C., Otten, W., Kravchenko, A., Balseiro-Romero, M., Beckers, É.,
584 Chalhoub, M., … & Kiryanyaz, S. (2018). Emergent properties of microbial

585 activity in heterogeneous soil microenvironments: Different research
586 approaches are slowly converging, yet major challenges remain. *Frontiers in*
587 *Microbiology*, *9*, 1929.
588 Burd, G. I., Dixon, D. G., & Glick, B. R. (2000). Plant growth-promoting bacteria
589 that decrease heavy metal toxicity in plants. *Canadian Journal of Microbiology*,
590 *46*(3), 237–245.
591 Carminati, A., Kaestner, A., Lehmann, P., & Flühler, H. (2008). Unsaturated
592 water flow across soil aggregate contacts. *Advances in Water Resources*,
593 *31*(9), 1221–1232.
594 de Weert, S., Vermeiren, H., Mulders, I. H. M., Kuiper, I., Hendrickx, N.,
595 Bloemberg, G. V., … Lugtenberg, B. J. J. (2002). Flagella-Driven Chemotaxis
596 Towards Exudate Components Is an Important Trait for Tomato Root
597 Colonization by *Pseudomonas fluorescens*. *Molecular Plant-Microbe*
598 *Interactions*, *15*(11), 1173–1180.
599 Dechesne, A., Bertolla, F., Grundmann, L., Lyon, C. B., & Icrobiol, A. P. P. L. E.
600 N. M. (2005). *Impact of the Microscale Distribution of a Pseudomonas Strain*
601 *Introduced into Soil on Potential Contacts with Indigenous Bacteria*. *71*(12),
602 8123–8131.
603 Ekschmitt, K., Liu, M., Vetter, S., Fox, O., & Wolters, V. (2005). Strategies used
604 by soil biota to overcome soil organic matter stability — why is dead organic
605 matter left over in the soil? *Geoderma*, *128*(1), 167–176.
606 Gupta Sood, S. (2003). Chemotactic response of plant-growth-promoting
607 bacteria towards roots of vesicular-arbuscular mycorrhizal tomato plants. *FEMS*
608 *Microbiology Ecology*, *45*(3), 219–227.
609 Hapca, S., Baveye, P. C., Wilson, C., Lark, R. M., & Otten, W. (2015). Three-
610 Dimensional Mapping of Soil Chemical Characteristics at Micrometric Scale by

611 Combining 2D SEM-EDX Data and 3D X-Ray CT Images. *PLOS ONE*, *10*(9),
612 e0137205.
613 Hassink, J., Bouwman, L.A., Zwart, K.B., Brussard, L. (1993). Relationships
614 between habitable pore space, soil biota and mineralization rates in grassland
615 soils. *Soil Biology and Biochemistry*, 25, 47–55.
616 Hayat, R., Ali, S., Amara, U., Khalid, R., & Ahmed, I. (2010). Soil beneficial
617 bacteria and their role in plant growth promotion: a review. *Annals of*
618 *Microbiology*, *60*(4), 579–598.
619 Houston, A. N., Otten, W., Baveye, P. C., & Hapca, S. (2013a). Adaptive-
620 window indicator kriging: A thresholding method for computed tomography
621 images of porous media. *Computers & Geosciences*, *54*, 239–248.
622 Houston, A. N., Schmidt, S., Tarquis, A. M., Otten, W., Baveye, P. C., & Hapca,
623 S. (2013b). Effect of scanning and image reconstruction settings in X-ray
624 computed microtomography on quality and segmentation of 3D soil images.
625 *Geoderma*, 207, 154–165.
626 Juyal, A., Eickhorst, T., Falconer, R., Baveye, P. C., Spiers, A., & Otten, W.
627 (2018). Control of Pore Geometry in Soil Microcosms and Its Effect on the
628 Growth and Spread of *Pseudomonas* and *Bacillus* sp. *Frontiers in*
629 *Environmental Sciences*, 6, 73, 1-12.
630 Juyal, A., Otten, W., Falconer, R., Hapca, S., Schmidt, H., Baveye, P. C., &
631 Eickhorst, T. (2019). Combination of techniques to quantify the distribution of
632 bacteria in their soil microhabitats at different spatial scales. *Geoderma*, *334*,
633 165–174.
634 Kizungu, R., Grundmann, G. L., Dechesne, A., Bartoli, F., Flandrois, J. P., &
635 Chasse, J. L. (2001). Spatial Modeling of Nitrifier Microhabitats in Soil ´,.
636 *Distribution*, *1709*, 1709–1716.

637 Kuzyakov, Y., & Blagodatskaya, E. (2015). Microbial hotspots and hot moments
638 in soil: Concept & review. *Soil Biology and Biochemistry*, *83*, 184–199.
639 Neal, A. L., Ahmad, S., Gordon-Weeks, R., & Ton, J. (2012). Benzoxazinoids in
640 root exudates of maize attract pseudomonas putida to the rhizosphere. *PLoS*
641 *ONE*, *7*(4), e35498.
642 Madigan, M. T., Clark, D. P., Stahl, D., & Martinko, J. M. (2010). *Brock biology*
643 *of microorganisms*. 13th ed. San Francisco: Benjamin Cummings.
644 Nunan, N., Wu, K., Young, I. M., Crawford, J. W., & Ritz, K. (2002). In situ
645 spatial patterns of soil bacterial populations, mapped at multiple scales, in an
646 arable soil. *Microbial Ecology*, *44*(4), 296–305.
647 Nunan, Naoise, Wu, K., Young, I. M., Crawford, J. W., & Ritz, K. (2003). Spatial
648 distribution of bacterial communities and their relationships with the micro-
649 architecture of soil. *FEMS Microbiology Ecology*, *44*(2), 203–215.
650 Portell, X., Pot, V., Garnier, P., Otten, W., & Baveye, P. C. (2018). Microscale
651 Heterogeneity of the Spatial Distribution of Organic Matter Can Promote
652 Bacterial Biodiversity in Soils: Insights From Computer Simulations. *Frontiers in*
653 *Microbiology*, 9, 1583.
654 Ruamps, L. S., Nunan, N., & Chenu, C. (2011). Microbial biogeography at the
655 soil pore scale. *Soil Biology and Biochemistry*, *43*(2), 280–286.
656 Schlüter, S., Henjes, S., Zawallich, J., Bergaust, L., Horn, M., Ippisch, O., &
657 Dörsch, P. (2018). Denitrification in soil aggregate analogues-effect of
658 aggregate size and oxygen diffusion. *Frontiers in Environmental Science, 6, 17*.
659 Schmidt, S., Bengough, A. G., Gregory, P. J., Grinev, D. V., & Otten, W. (2012).
660 Estimating root-soil contact from 3D X-ray microtomographs. *European Journal*
661 *of Soil Science, 63*(6), 776-786.
662 Strong, D. T., De Wever, H., Merckx, R., & Recous, S. (2004). Spatial location

663 of carbon decomposition in the soil pore system. *European Journal of Soil*
664 *Science*.
665 Vieublé Gonod, L., Chadoeuf, J., & Chenu, C. (2006). Spatial distribution of
666 microbial 2, 4-dichlorophenoxy acetic acid mineralization from field to
667 microhabitat scales. *Soil Science Society of America Journal*, *70*(1), 64-71.
668 Young, I. M., Crawford, J. W., Nunan, N., Otten, W., & Spiers, A. (2008).
669 Microbial distribution in soils: physics and scaling. *Advances in agronomy*, *100*,
670 81-121.
671 Zaidi, A., Khan, M. S., Ahemad, M., & Oves, M. (2009). Plant growth promotion
672 by phosphate solubilizing bacteria. *Acta Microbiologica et Immunologica*
673 *Hungarica,56*(3), 263-284.
674 Zhuang, X., Chen, J., Shim, H., & Bai, Z. (2007). New advances in plant
675 growth-promoting rhizobacteria for bioremediation. *Environment International,*
676 *33*(3), 406-413.
677
678
679
680

681 **Figure legends**

682

683 **Figure 1:** Schematic representation of a soil thin section (vertical cut) used for
684 the enumeration of microbial cells within the soil matrix.

685

686 **Figure 2:** Example of alignment of a stereomicroscopic image (a) with a CT
687 image (b). The circle in the middle is the glass bead representing the point of
688 bacteria inoculation. Sample packed at bulk density of 1.3 g cm^{-3}. The red

689 frame represents the area used for analysis of both cell counts and pore space
690 analyses. Scale bar: 5 mm.
691
692 **Figure 3:** Microscopic images of DAPI-stained *Pseudomonas fluorescens* cells
693 in thin sections of soil microcosms packed at (a) 1.3 g cm^{-3} and (b) 1.5 g cm^{-3}
694 bulk density. Bacterial cells are bright blue. Scale bar: 20 µm.
695
696 **Figure 4:** Distribution of bacterial cells in vertical thin sections of resin
697 impregnated soil microcosms with inoculum (*Pseudomonas fluorescens*). Left
698 (a+c): Soil microcosm packed at bulk density of 1.3 g cm^{-3}; right (b+d): Soil
699 microcosm packed at bulk density of 1.5 g cm^{-3}. Top (a+b): Soil thin section
700 passing through the glass bead; bottom (2): Soil thin section approx. 2.5 mm
701 above the glass bead. 1st column: bottom of the packed soil microcosm; 9th
702 column: top of the packed soil microcosm. Unit of cell densities: cells per mm^2.
703 GB: glass bead. 1 square represents a distance of 1×1 mm.
704
705
706 **Figure 5:** Cell densities of *Pseudomonas fluorescens* cells in soil thin sections
707 based on the distance from the glass bead. a: packed at bulk density of 1.3 g
708 cm^{-3}; b: packed at bulk density of 1.5 g cm^{-3}. Each data point in the graph
709 represents one counting spot analysed in each replicate of a thin section.
710
711 **Figure 6:** Relationship of *Pseudomonas fluorescens* cell density with soil
712 porosity (a+b), connectivity (c+d), and solid-pore interface (e+f) in soil thin
713 sections packed at bulk density of 1.3 g cm^{-3} (left) and 1.5 g cm^{-3} (right). Each

714 data point in the graph represents one counting spot analysed in each replicate
715 of a thin section.
716

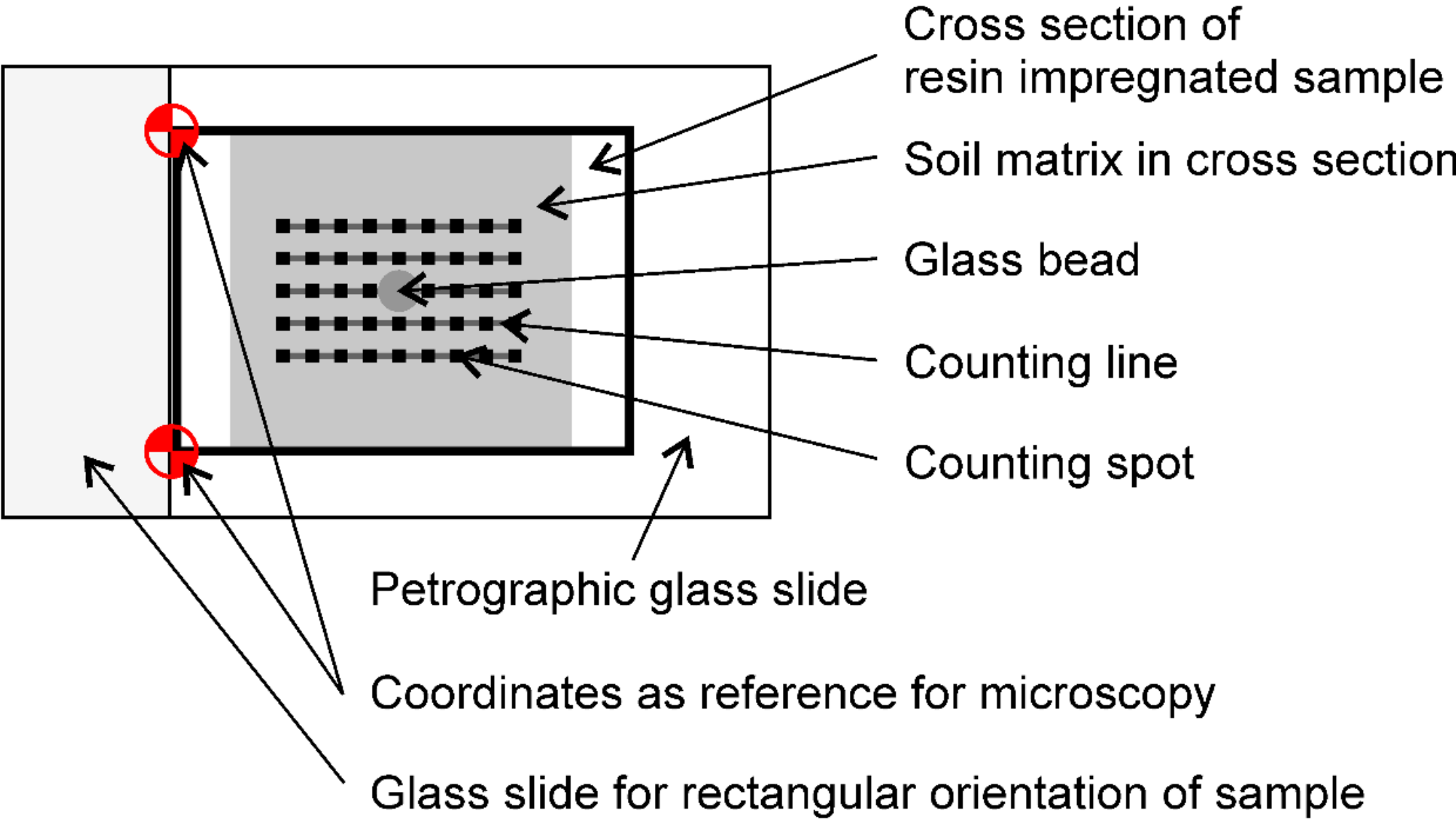
Cross section of
resin impregnated sample
Soil matrix in cross section
Glass bead
Counting line
Counting spot
Petrographic glass slide
Coordinates as reference for microscopy
Glass slide for rectangular orientation of sample

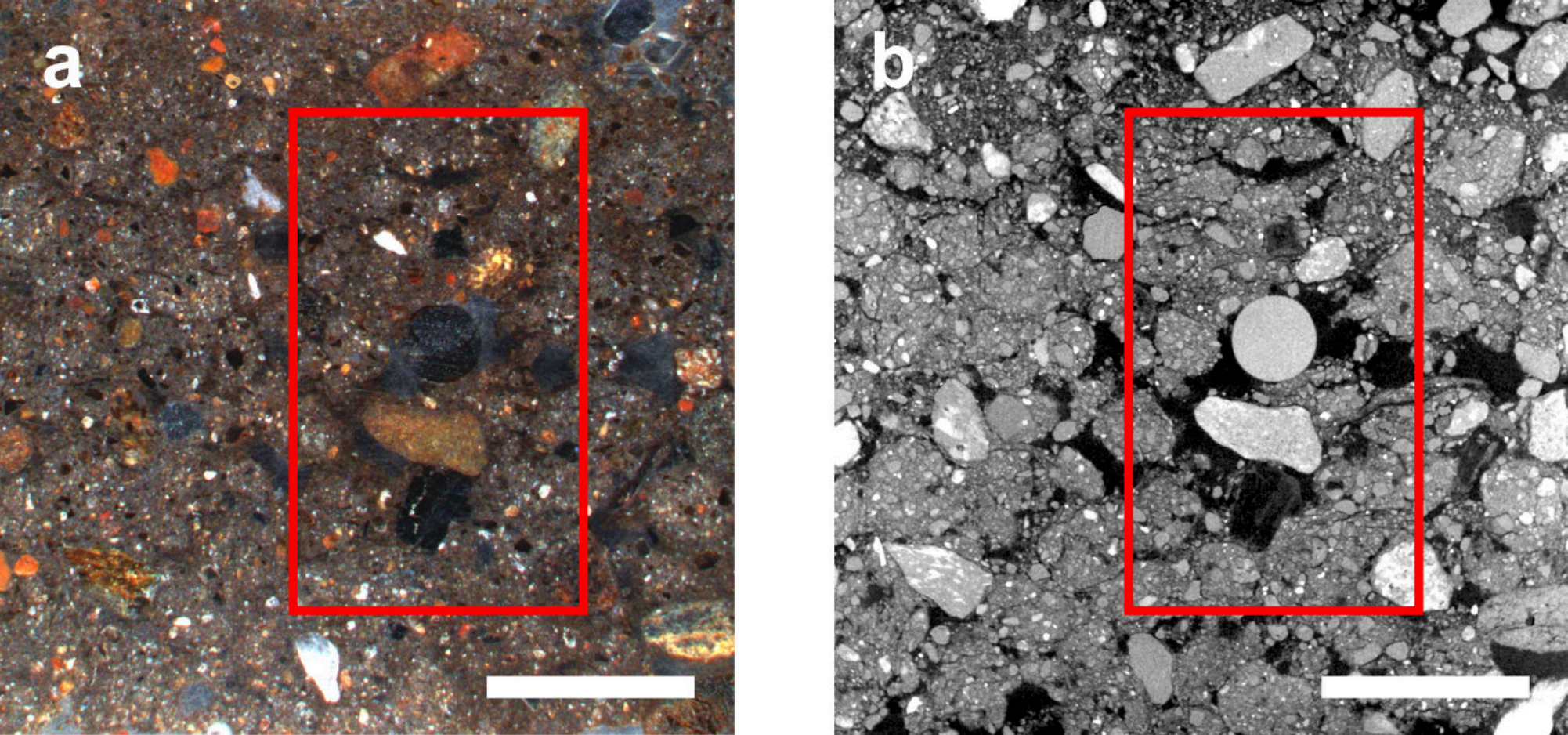
a
b

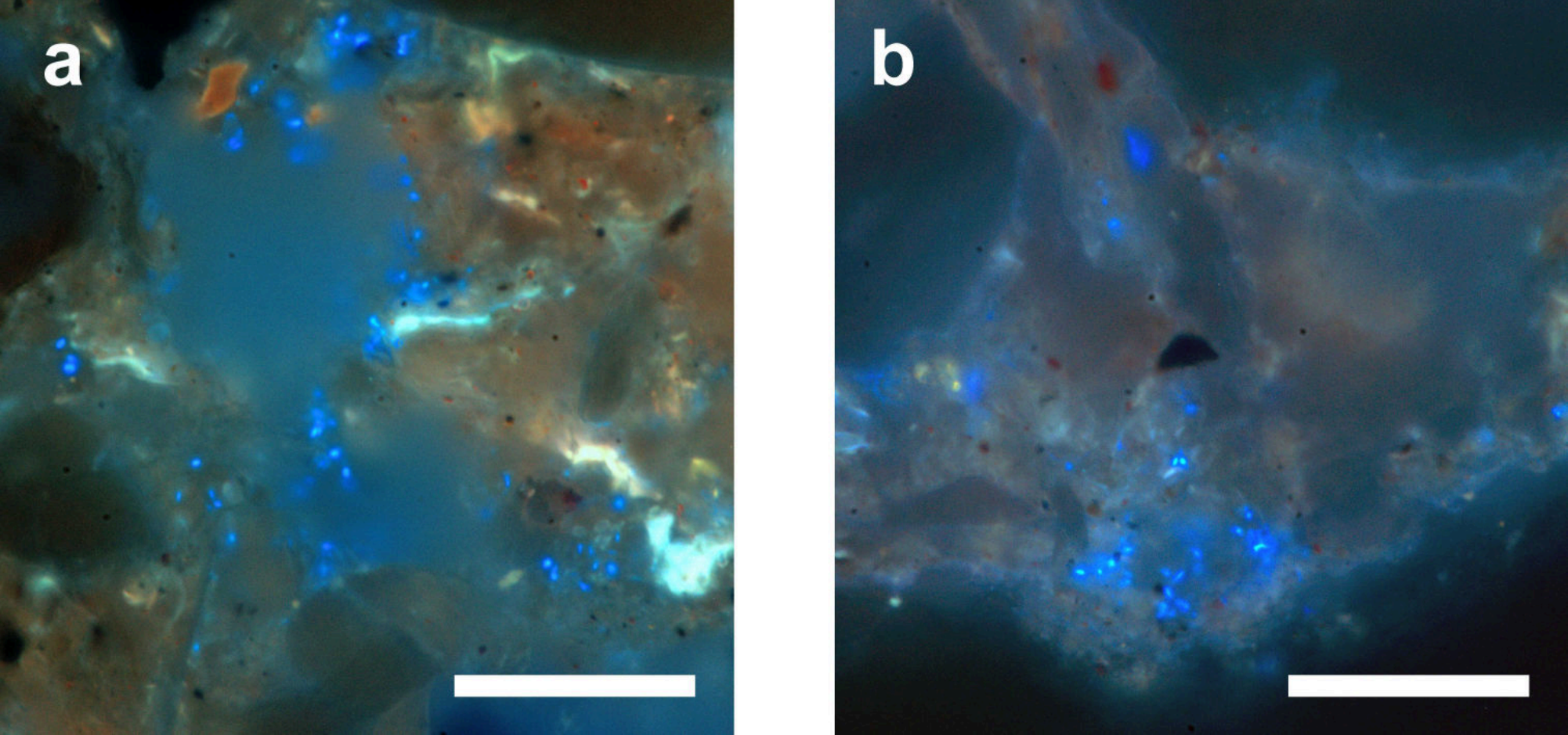
a
b

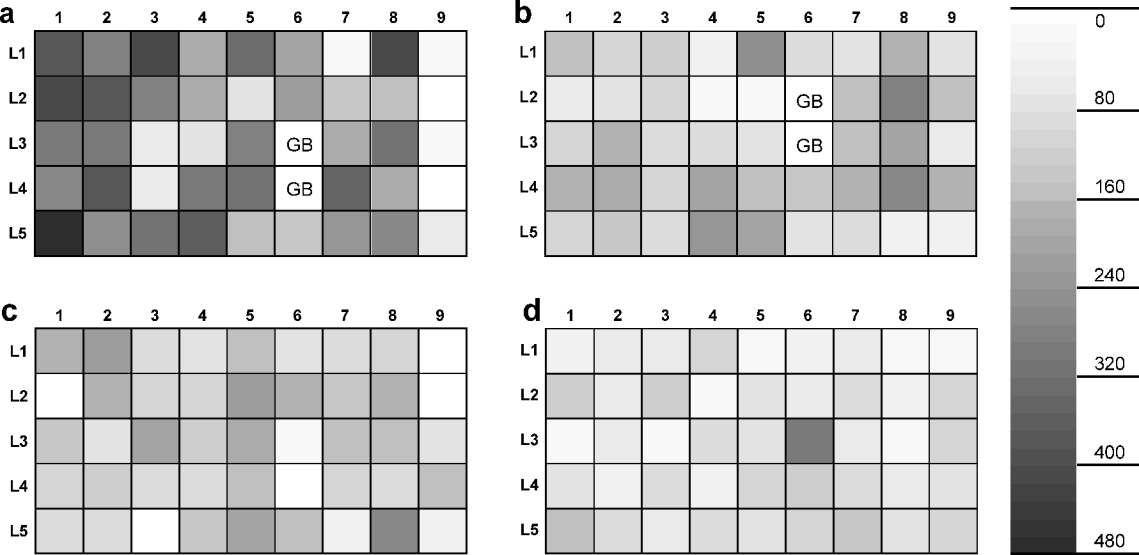
a
1 2 3 4 5 6 7 8 9
L1
L2
L3
GB
L4
GB
L5
b
1 2 3 4 5 6 7 8 9
L1
L2
GB
L3
GB
L4
L5
c
1 2 3 4 5 6 7 8 9
L1
L2
L3
L4
L5
d
1 2 3 4 5 6 7 8 9
L1
L2
L3
L4
L5
0
80
160
240
320
400
480

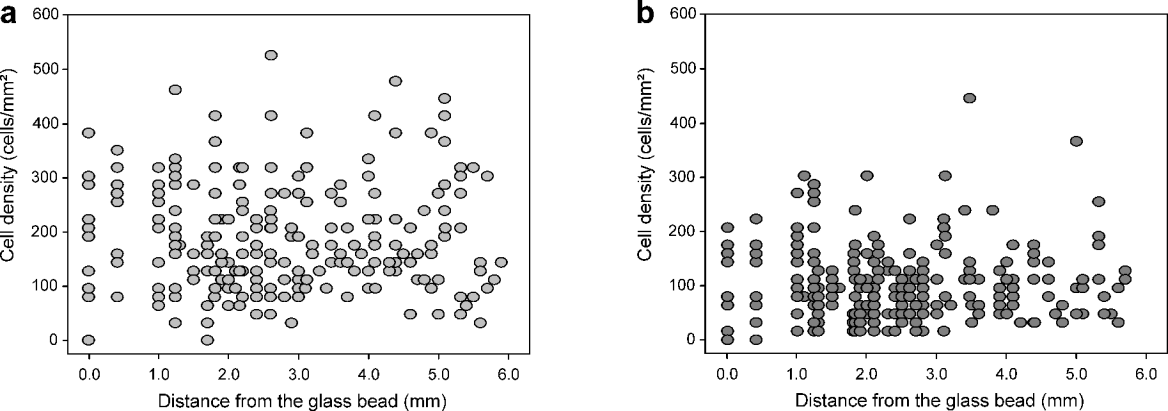
a
b
Cell density (cells/mm²)
Distance from the glass bead (mm)
0
100
200
300
400
500
600
0.0
1.0
2.0
3.0
4.0
5.0
6.0

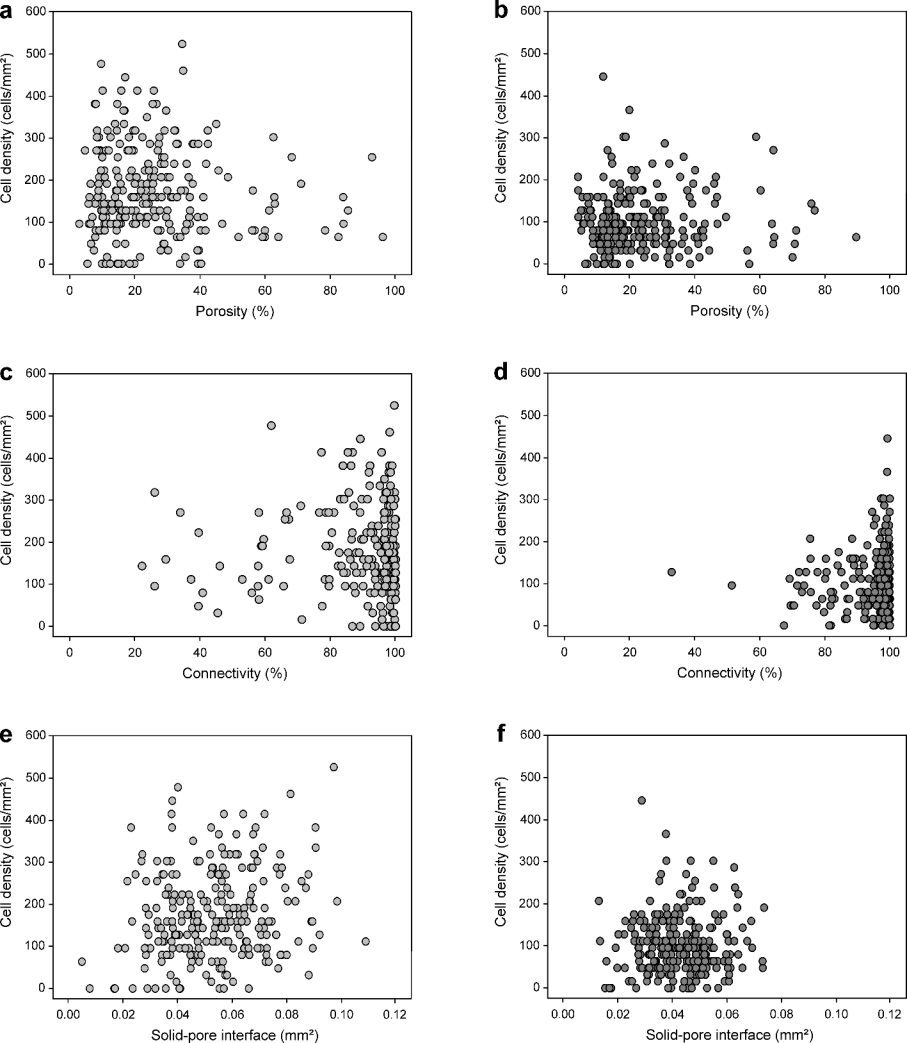
a
b
c
d
e
f
Cell density (cells/mm²)
Porosity (%)
Connectivity (%)
Solid-pore interface (mm²)
0
100
200
300
400
500
600
0
20
40
60
80
100
0.00
0.02
0.04
0.06
0.08
0.10
0.12

Tables MS Juyal et al., submitted to EJSS

Table 1: Results of the Poisson model analysis on influence of distance to the bead on the spread of *Pseudomonas fluorescens* cells in soil with different bulk-density treatments. Numbers reported in the table are the *p*-values and coefficient values (β) are the estimation of the fixed coefficients of distance in the test model of the analysis.

Treatments	*p*-value	Coefficient β
Pseudomonas fluorescens inoculated in soil packed at bulk density 1.3 g cm^{-3}	0.002	3.122
Pseudomonas fluorescens inoculated in soil packed at bulk density 1.5 g cm^{-3}	0.447	-0.762

Table 2: Results of the Poisson model analysis on influence of pore structure on the spread of *Pseudomonas fluorescens* cells in soil with different bulk-density treatments. Numbers reported in the table are the *p*-values and coefficient values (*β*) are the estimation of the fixed coefficients (porosity, connectivity and solid-pore interface) in the test model of the analysis.

Treatments	Porosity		Connectivity		Solid-pore interface	
	***p*-value**	**Coefficient *β***	***p*-value**	**Coefficient *β***	***p*-value**	**Coefficient *β***
Pseudomonas fluorescens inoculated in soil packed at bulk density 1.3 g cm^{-3}	0.147	-1.453	0.001	-3.274	0.000	5.999
Pseudomonas fluorescens inoculated in soil packed at bulk density 1.5 g cm^{-3}	0.222	1.225	0.111	2.571	0.302	1.034

Influence of soil structure on the spread of *Pseudomonas fluorescens* in soil at microscale

Archana Juyal[1, 2, 3], Wilfred Otten[1, 4], Philippe C. Baveye[5], Thilo Eickhorst[2]*

[1] School of Science Engineering and Technology, Abertay University, Dundee, UK.
[2] FB 2 (Biology/Chemistry), University of Bremen, Bremen, Germany.
[3] Department of Plant, Soil and Microbial Sciences, Michigan State University, Michigan, USA.
[4] School of Water, Energy and Environment, Canfield University, Cranfield, UK.
[5] ECOSYS Unit, AgroParisTech, Université Paris-Saclay, Avenue Lucien Brétignières, 78850 Thiverval-Grignon, France.
* eickhorst@uni-bremen.de

Supplementary information

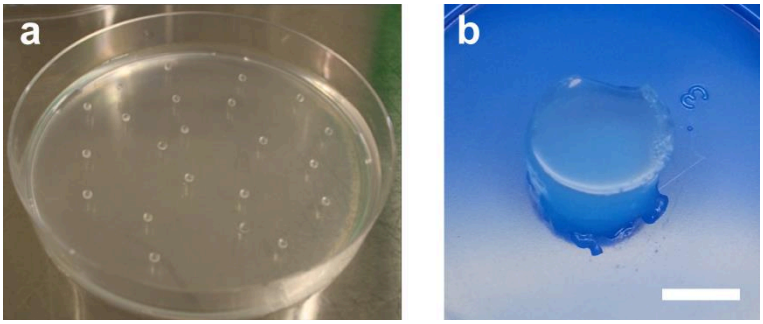

Figure_1_Supp: Preparation of agarose pellets for inoculation in soil. a: Glass beads on a layer of LMP-agarose containing a bacterial suspension of *Pseudomonas fluorescens* cells. b: Agarose pellet of size 3.5 mm in diameter and ca.4 mm in height containing *Pseudomonas fluorescens* cells and a glass bead in the center. Scale bar: 2 mm.

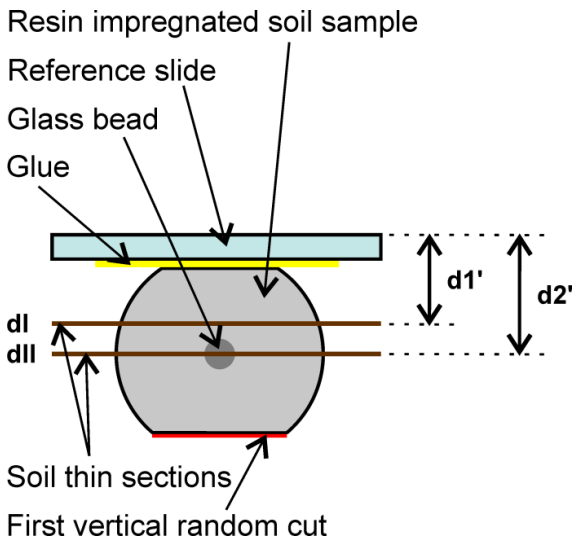

Figure_2_Supp: Preparation of soil thin sections from resin impregnated soil samples. View on top of the sample. Distances for the correlation with CT-data are measured between the reference slide and the cuts for the thin sections.

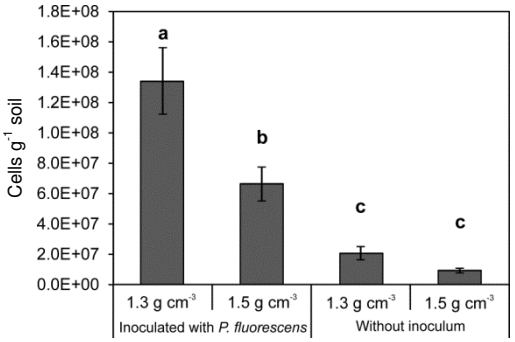

Figure_3_Supp: Bacterial cell counts (DAPI) on soil thin sections derived from soil microcosms packed at different bulk densities. Enumerated cell densities extrapolated to cells per g soil. Letters indicate significant differences (p<0.05); error bars: SE (n=3).

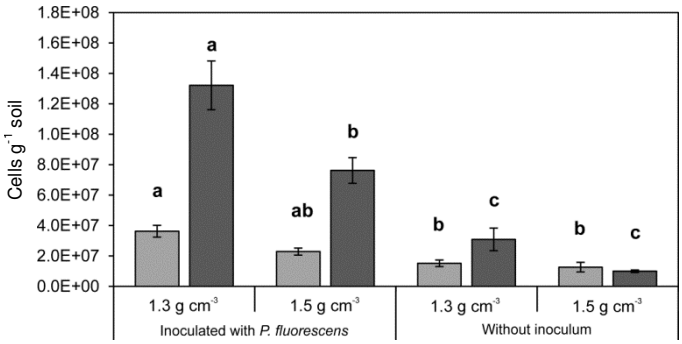

Figure_4_Supp: Bacterial cell counts (CARD-FISH) from soil microcosms packed at different bulk densities. Light grey: 1 day after packing and incubation; dark grey: 14 days after packing and incubation. Enumerated in soil suspensions and extrapolated ti cells per g soil. Letters indicate significant differences (p<0.05); error bars: SE (n=3).

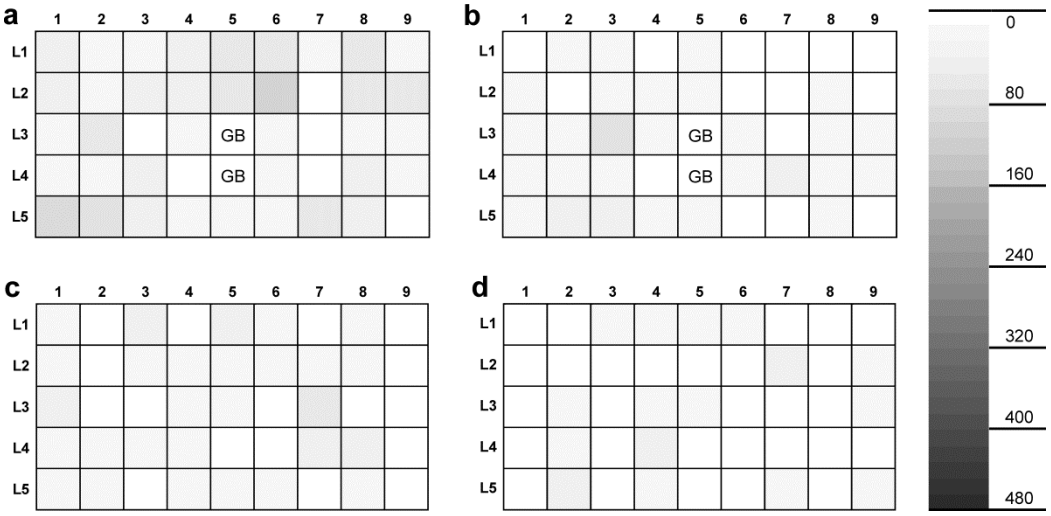

Figure_5_Supp: Distribution of bacterial cells in vertical thin sections of resin impregnated soil microcosms without inoculum (control). Left (a, c): Soil microcosm packed at bulk density of 1.3 g cm^{-3}; Right (b, d): Soil microcosm packed at bulk density of 1.5 g cm^{-3}. Top (a, b): Soil thin section passing the glass bead; bottom (c, d): 1st column: bottom of the packed soil microcosm; 9th column: top of the packed soil microcosm. Soil thin section approx. 2.5 mm above the glass bead. Unit of cell densities: cells per mm². GB: glass bead. 1 square represents a distance of 1×1 mm.

Table_1_Supp: Mean values of pore characteristics in soil packed at bulk-density 1.3 and 1.5 g cm^{-3}. Mean values ±SE are presented (*n*=3).

Bulk-density (g cm^{-3})	**Porosity (%)**	**Connectivity (%)**	**Soil-pore interface (mm^2)**
1.3	24 ±1.05	94 ±0.55	0.05 ±0.001
1.5	23 ±0.91	89 ±0.99	0.04 ±0.001